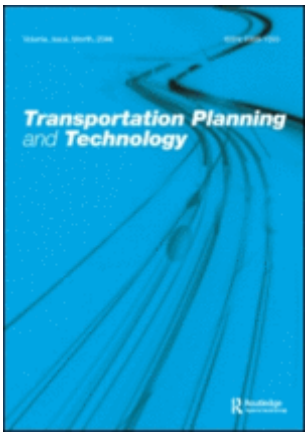

Macro modelling of traffic flow using continuous timed Petri nets

Journal:	*Transportation Planning and Technology*
Manuscript ID	Draft
Manuscript Type:	Original Article
Date Submitted by the Author:	n/a
Complete List of Authors:	Ferreira, Cláudia; Universidade de Lisboa Instituto Superior Tecnico, Neves, Luís; University of Nottingham Faculty of Engineering
Keywords:	Continuous timed Petri nets, Freeway traffic, Hybrid model, Simulation, Calibration, Validation

Macro modelling of traffic flow using continuous timed Petri nets

Cláudia Ferreira[a]* and Luís Canhoto Neves[b]

a CERIS, Instituto Superior Técnico (IST) - University of Lisbon, Av. Rovisco Pais, 1049-001, Lisbon, Portugal, e-mail: claudiaarferreira@tecnico.ulisboa.pt

b Resilience Engineering Research Group, University of Nottingham, Nottingham, UK, e-mail: luis.neves@nottingham.ac.uk

* Corresponding author

Acknowledgements

The authors gratefully acknowledge the support of FCT (Portuguese Foundation for Science and Technology) through program SFRH/BD/88195/2012.

Macro modelling of traffic flow using continuous timed Petri nets

Word count: 7563 words

Abstract:

In this paper, continuous timed Petri nets (CTPN) are used to develop a hybrid traffic model, where the network is modelled as a macroscopic model calibrated by microscopic models. The concept of CTPN is used to build a modular model, where first the highway traffic system is decomposed into several systems, based on structural entities (i.e. highway segment, on- and off-ramp links), which are coalesced into a complete model. The result is a light, versatile and easily scalable stochastic model for traffic flow. The calibration and validation of the traffic model was performed through the comparison of the basic traffic parameters (flow rate, density, and mean speed) obtained through the traffic model implemented and the commercial micro-modelling software, Aimsun, for part of Portugal's highway network. The results show that the proposed methodology results in a good trade-off between accuracy, simplicity, and computational cost.

Keywords: Continuous timed Petri nets; Freeway traffic; Hybrid model; Simulation; Calibration; Validation

1 Introduction

Traffic flow can be considered a heterogeneous system, with two forms of behaviour: continuous and discrete (Tolba *et al*., 2005). The traffic flow takes a continuous behaviour in uninterrupted-flow facilities, like freeways and highways. In this type of facilities, the traffic flow conditions result from the interaction among vehicles in the traffic stream and the characteristics (geometric and environmental) of the roadway. While in interrupted-flow facilities, the traffic flow is carried out in a discrete form. Interrupted-flow facilities are access points that can stop the traffic periodically (or slow it significantly), like signalized and unsignalized intersections (HCM, 2010).

The adoption of traffic models is of paramount importance for the design, prediction and control of traffic systems (Julvez and Boel, 2010; Ferrara *et al*., 2018). In the literature, the dynamics of vehicles and their interaction in freeways can be described through three types of traffic models: microscopic, mesoscopic and macroscopic. This classification is made according to the level of detail of the traffic models, corresponding to the following cases (Ferrara *et al*., 2018): (a) microscopic models: the dynamics of all vehicles and their interactions are represented in detail, each vehicle is described with a dynamic model, with different parameters (e.g., the desired speed or acceleration capabilities of the vehicle, as well as, the aggressiveness and reaction times of the driver); (b) macroscopic models: the traffic dynamics are represented at an aggregate level, being the flow of vehicles seen as a unique stream, in analogy with the flow of fluids, and its dynamics are described by means of aggregate variables, such

as flow rate, density and mean speed; (c) mesoscopic models: present an intermediate level of detail, do not distinguish individual vehicles but represent the heterogeneity of the drivers' choices in probabilistic terms.

Microscopic models are very detailed and, consequently, the computational effort can be exceptionally high when modelling large road networks. On the other hand, macroscopic models are less computationally intensive and can be used to model large road networks with an acceptable computational load. However, this computational advantage is balanced by their inability to capture some specific traffic phenomena related to the behaviour of individual drivers. In general, it is simpler to calibrate macroscopic models than microscopic models, since the former are characterised by fewer parameters (Ferrara *et al*., 2018). For these reasons, the use of macroscopic models is the most suitable choice when real-time applications are considered or large traffic networks are involved (Ferrara *et al*., 2018).

Petri Nets (PN) are a powerful modelling formalism, successfully used, in the last years, in different applications domains (Cheng *et al*., 2013; Latorre-Biel *et al*., 2017; Eisenberger and Fink, 2017; Kim and Yang, 2018; Si *et al*., 2018; Herajy *et al*., 2018; Ferreira *et al*., 2019). Concerning the field of transportations, Petri nets have been proven a powerful modelling tool to represent traffic networks either continuous-time systems (for instance, road stretches leading to a crossing and parts of freeway containing on/off-ramps (Tolba *et al*., 2005; Fanti *et al*., 2012)) or discrete-event systems (for example, accidents, critical weather conditions and signalized and unsignalized intersections (DiFebbraro and Sacco,2004; Dotoli and Fanti, 2006)). The use of Petri nets in traffic control modelling and analysis can be dated back to Jensen (1986), who first proposed the use of coloured Petri nets to model traffic lights. Later, Giua (1991) applied Petri nets to model traffic networks. DiFebbraro and Sacone (1998) used Hybrid Stochastic Petri net to model a freeway system, in which the vehicle flow behaviour is represented by a continuous-time model, whereas the changes in the system behaviour are modelled as discrete events. Since then a range of authors have proposed different models for traffic analysis based on PN: Di Febbraro and Sacco (2004); Tolba *et al*. (2005); Zhang *et al*. (2008); Julvez and Boel (2010); Dotoli *et al*. (2011); Fanti *et al*. (2012, 2014); Di Febbraro *et al*. (2016). In this paper, a continuous timed Petri net (CTPN), rather than the original Petri net, is used to model traffic. CTPN are the result of relaxing discrete nets by removing the integrality constraint in the firing of transitions. In contrast to discrete Petri nets, the state of a continuous Petri net is a vector of non-negative real numbers and the firing of the transitions are real valued flows of material/cars that pass from the input places to the output places (Tolba *et al*., 2005; Julvez and Boel, 2010). These are used to develop a hybrid traffic model. In this model, the road network is modelled as a macroscopic model, but each segment is calibrated as a microscopic model. The road network is decomposed into several segments, based on structural entities (i.e. highway segments, on- and off-ramp links). The calibration is performed for each segment, while the macro simulation allows to model large road networks. To achieve this, a methodology based on the

works of Tolba *et al*., (2005) and Fanti *et al*. (2012, 2014) is proposed herein. The original model is enhanced to improve the quality of the fit to results obtained through the commercial micro-modelling software, Aimsun (Aimsun, 2019). For that, two new parameters are introduced: correction factor of the critical density, c_1; and critical speed, S_{cri}. The calibration and validation of the traffic model is performed through the comparison of the basic traffic parameters (flow rate, density, and mean speed) obtained through the traffic model implemented and the commercial micro-modelling software, Aimsun (Aimsun, 2019).

The outline of this paper is as follows: in Section 2, the fundamental properties of Petri nets are described; Section 3 introduces the methodology of the traffic model implemented; the results and discussion are presented in Section 4 and conclusions are drawn in Section 5.

2 Petri nets

A Petri net is a bipartite weighted directed graph composed by four basic elements: places, transitions, arcs and tokens. Places are a type of nodes of the network symbolising a specific state or condition of the system, whereas transitions symbolise the triggering of events or actions and are the second type of node. Both nodes are linked by directed arcs. An arc connects a place with a transition, or vice-versa. Lastly, tokens are stored in places, representing the present state of the system, and their distribution over the places is called the marking of the network, M (Peterson, 1977; Murata, 1989; Schneeweiss, 2004). The initial state of the system is defined by the initial marking, M_0.

Figure 1 shows a simple Petri net model. The net is composed of three places (denoted by circles), one transition (represented by a rectangle) and tokens (illustrated by dots) within the places. Places and transitions are connected by arrows that indicate the direction the tokens should move. The movement of the tokens between places and the evolution of the system from one state to another is governed by the firing of transitions. A transition is enabled to fire when the number of tokens in all input places is greater than or equal to the weight of the pre-condition arcs (arrows that link the input places to the transitions). These two elements (tokens and transitions) are responsible for modelling the dynamic behaviour of the system.

In Figure 1, places p_1 and p_2 are the input places of transition t_1, while place p_3 is the output place. Transition t_1 is enabled to fire once the pre-conditions are verified (i.e., at least one token in p_1 and two tokens in p_2), Figure 1(a). After the transition fires, the weight of tokens of the pre-conditions are removed from the respective input places, and the weight of tokens of the post-conditions are added to the respective output place, Figure 1(b).

A continuous timed Petri net is an extension of the original of Petri nets (David and Alla, 2010). In a timed Petri net, there is a delay between enabling and firing, and the marking of a place is made through

an integer number and the firing of a transition occurs at discrete times while, in a CTPN, the marking of a place becomes a non-negative real number and the firing of a transition becomes a continuous flow. The CTPN was obtained as a relaxation of the discrete Petri nets and this formalism is useful for modelling continuous system such as handling of fluids (Alla and David, 1998) or traffic flows (Tolba *et al*., 2005). Pictorially, in a CTPN, a place is denoted by a double circle and a transition by a double rectangle.

3 Traffic model description

The traffic model implemented herein is based on the works of Tolba *et al*. (2005) and Fanti *et al*. (2012, 2014). The concept of continuous times Petri net is used to build a modular model to describe a highway traffic system. It is a bottom-up approach, where first the highway traffic system is decomposed into several systems, based on structural entities (i.e. highway segments, on- and off-ramp links), and after that sub-models are coalesced into a complete model, representing the whole system (Fanti *et al*., 2014).

The highway traffic system consists of 5 sub-modules: generic highway segment, origin segment, on- and off-ramp links, and destination segment. Each sub-module is described in the following points.

3.1 Generic highway segment model

In this methodology, it is assumed that a highway network is discretized into smaller highway segments with length, L, between 100 – 3000 m, with a maximum vehicle capacity, C. Figure 2 illustrates the Petri net scheme for two generic highway segments of length L_i and L_{i+1}. Each highway segment is modelled by two places and one transition. The places model the highway segment, while the transition stands for the separation between the segments i and $i+1$. The marking $m^v_i(t)$ of place p^v_i denotes the number of vehicles in highway segment i, the marking $m^a_i(t)$ of place p^a_i correspond to the number of available spaces in the highway segment i, and $v_i(t)$ stands for the transition firing speed that represents the average flow rate $q_i(t)$ of the highway segment i (Tolba *et al*., 2005; Fanti *et al*., 2014).

Regarding Figure 2, vehicles that enter in segment $i+1$ are modelled by transition t_i and vehicles that exit from segment $i+1$ are modelled by transition t_{i+1}. When the transition t_i fires, the number of vehicles that exit from segment i, $v_i(t)$, is subtracted from places p^v_i and p^a_{i+1} and added to places p^a_i and p^v_{i+1}, modelling, in this way, the number of vehicles transiting from place p^v_i to place p^v_{i+1} and the number of available spaces in each segment after the transition.

The transition firing speed, $v_i(t)$, is a piecewise linear function of the network marking, depending not only on the marking of the place p^v_i (i.e. on the number of the vehicles in the upstream segment i) but

also on the marking of the place p^a_{i+1} (i.e. the number of spaces available in the downstream segment $i+1$) (Tolba *et al*., 2005):

$$v_i(t) = v_{max,i} \times \min\left[\alpha_i, m_i^v(t), C_{i+1} - m_{i+1}^v(t)\right] \quad (1)$$

where $v_{max,i}$ represents for the maximum firing frequency of transition t_i and is given by:

$$v_{max,i} = \frac{S_{free,i}}{L_i} \quad (2)$$

where $S_{free,i}$ the maximum speed, and α_i and C_i correspond, respectively, to the maximum number of possible simultaneous firings for transition t_i and the limited capacity of place p^v_i. Both variables are related to the traffic parameters according to:

$$\alpha_i = \frac{q_{max,i} \times L_i}{S_{free,i}} \quad (3)$$

$$C_i = \rho_i \times C_i \quad (4)$$

where $q_{max,i}$ represents the maximum flow rate, and ρ_i the jam density in highway segment i.

The conservation of the number of vehicles in segment i is expressed as (Tolba *et al*., 2005):

$$\frac{dm_i^v(t)}{dt} = v_{i-1}(t) - v_i(t) \quad (5)$$

This differential equation is responsible for the marking evolution of the place p^v_i in the traffic model. Furthermore, each highway segment has marking invariants (Tolba *et al*., 2005):

$$m_i^v(t) + m_i^a(t) = C_i \quad \forall t \geq 0 \quad (6)$$

The remain macroscopic parameters of the traffic flow model, average flow density $\rho_i(t)$ and average speed $S_i(t)$ for highway segment i, are given by (Tolba *et al*., 2005):

$$\rho_i(t) = \frac{m_i^v(t)}{L_i} \quad (7)$$

$$S_i(t) = \frac{v_i(t) \times L_i}{m_i^v(t)} \quad (8)$$

3.2 Origin segment model

The Petri net model for the origin segment is shown in Figure 3. The origin segment is modelled by place p_i and transition t_i, and models the number of vehicles that enter in the network in each instant. Each input point of the network has associated an origin segment.

The transition firing speed, $v_i(t)$ given by:

$$v_i(t) = \min\left\{f_i(t), v_{max,i} \times \left[C_{i+1} - m^v_{i+1}(t)\right]\right\} \quad (9)$$

where $f_i(t)$ is the traffic flow that wants to enter in the network in each instant. The traffic flow that wants to enter the network is not constant over time and, in this model, it was considered that $f_i(t)$ follows an exponential distribution.

3.3 On-ramp model

The Petri net submodel for the on-ramp is shown in Figure 4. Transition t_{on} models the input of vehicles from the ramp to the network, being the vehicles routed from the ramp, of length L_{on}, to the highway segment $i+1$ by the arc from transition t_{on} to place p^v_{i+1} and by the arc from place p^a_{i+1} to transition t_{on}. Moreover, the marking $m^v_{on}(t)$ of place p^v_{on} represents the number of vehicles in ramp, and the marking $m^a_{on}(t)$ of place p^a_{on} the number of available spaces in ramp (Fanti *et al*., 2014).

As can be seen, in the on-ramp model the highway segment $i+1$ have input traffic flow from two different segments: highway segment i and on-ramp. The transition firing speed of the highway segment i, $v_i(t)$, is given by Equation 1, while the transition firing speed of the on-ramp, $v_{on}(t)$, is expressed by:

$$v_{on}(t) = v_{max,on} \times \min\left[\alpha_{on}, m^v_{on}(t), C_{i+1} - m^v_{i+1}(t)\right] \quad (10)$$

where $v_{max,on}$ represents the maximum firing frequency and α_{on} the maximum number of possible simultaneous firing of transition t_{on}.

In interrupted traffic flow conditions, in an on-ramp, it is assumed that the ratio of vehicles entering each segment is proportional to the maximum firing frequency, v_{max}, in each of them (Equations 1 and 10). The time interval discretization should be defined to ensure that, in each time step, it is not possible for more vehicles to enter than the available space in a given segment. For this case study, in the most unfavourable situation, the maximum firing frequency, $v_{max,i}$, is 0.33 s^{-1} (Equation 2, where $S_{free,i}$ = 120 km/h is the maximum speed and L_i = 100 m the shorter segment length). Since there are two segments in an on-ramp, a maximum of 66% of the available spacer are occupied in each time step, guaranteeing that the number of vehicles entering a segment is lower than the number of available spaces.

In the on-ramp model, the marking invariant (see Equation 6) must be verified. The number of vehicles entering segment $i+1$ is never higher than the number of available spaces in the segment. In the situation of congestion, the number of vehicles that merge in the highway from each input segment is determined taking into account the number of available spaces and the maximum firing frequency.

3.4 Off-ramp model

The off-ramp model is very similar to the on-ramp model and is illustrated in Figure 5. In this situation, the transition t_{off} models the output of vehicles from the network to the ramp, being the vehicles routed from the highway segment i to the ramp, of length L_{off}, by the arc from place p^v_i to transition t_{off} and by the arc from transition t_{off} to place p^a_i (Fanti *et al*., 2014).

In the off-ramp model, the highway segment i have two output segments: highway segment $i+1$ and off-ramp. In this case, the transition firing speed, $v(t)$, to each segment is weighted by the vehicle fraction that leaves at each ramp:

$$v_i(t) = v_{max,i} \times \min\left[\alpha_i, m_i^v(t), C_{i+1} - m_{i+1}^v(t)\right] \times OD_i \quad (11)$$

$$v_{off}(t) = v_{max,i} \times \min\left[\alpha_i, m_i^v(t), C_{off} - m_{off}^v(t)\right] \times OD_{off} \quad (12)$$

where OD_{off} and OD_i are, respectively, the percentage of vehicles that leaves the highway by the off-ramp and the continue in the highway obtained from the Origin-Destination matrix, and C_{off} - m^v_{off} the number of available spaces in off-ramp segment.

3.5 Destination segment model

The Petri net for the destination segment is illustrated in Figure 6. The destination segment is just modelled by place p^v_i, and has the function of storing all the vehicles that leave the network. Each output point of the network has associated a destination segment.

In the highway segments that precede the destination segments, the Equation 1 can be simplified to:

$$v_{i-1}(t) = v_{max,i-1} \times \min\left[\alpha_{i-1}, m_{i-1}^v(t)\right] \quad (13)$$

4 Calibration and validation of the traffic model

Since the implemented traffic model is a macroscopic model, its calibration and validation are performed by comparing the values of the basic traffic parameters (speed, density, and flow rate) with results of the commercial micro-modelling software, Aimsun. The calibration of the model focuses on the adjustment of the basic traffic parameters in order to fit the local conditions, while validation focuses on demonstrating the ability of Petri nets to replicate the results obtained from traffic microsimulation tools (Toledo *et al*., 2003).

4.1 Case study

The case study presented in Figure 7 is located on the A1 highway in the locality of Vila Franca de Xira (VFXira). The analysis focus on the South to North flow, which has two input points (South and VFXira), and two output points (North and VFXira). The characteristics of the network presented in Table 1, were defined based on the information present in the Highway Capacity Manual (HCM, 2010). This network was chosen, mainly, since it is part of the highest traffic highway in Portugal, where total congestion is common.

The Petri net modelling the traffic on the network is illustrated in Figure 8. It is composed by nine highway segments of variable length (three highway segments, one off-ramp segment, one on-ramp segment, two origin segments, and two destination segments), fourteen places, and eight transitions. The origin and destination segments are considered as having zero length. The length of the remain segments is shown in Table 1.

4.2 Calibration

The calibration of the traffic model is performed by analysing the relation between the basic traffic parameters (speed, density, and flow rate) for the proposed model and a well-established microscopic model. In order to analyse all possible behaviours in the network, three case studies are considered:

- Case study A – The traffic flow on the highway (Sections 1, 2, and 3) is continuously increased until the situation of congestion, being the traffic flow on the on- and off-ramp null. This case study allows studying traffic patterns in continuous highway segments;
- Case study B – Increase the traffic flow in segment South – VFXira (Section 4), for constant traffic flows on the main road (Sections 1, 2, and 3). This case study allows studying traffic patterns in off-ramp segments (Section 4), and in the segment that precedes the bifurcation (Section 1);
- Case study C – Increase the traffic flow in segment VFXira – North (Section 5), for constant traffic flows on the main road (Sections 1, 2, and 3). This case study allows studying traffic patterns in on-ramp segments (Section 5), in the segments that precedes the junction (Sections 1, and 2), and in the segment that follows the junction of the two flows (Section 3).

For the five sections, the relationships between speed, density, and flow rate for the traffic model implemented was computed through the methodology described above, for a generic segment with a length of 1000 m and the network characteristics presented in Table 1. Each sample has a simulation time of 3 hours in order to ensure that the traffic flow is fully developed, with the data to be recorded every 10 minutes in each section.

4.2.1 Case study A: Highway segments

In Figure 9, the results obtained for the Sections 1, 2, and 3 using the traffic model implemented are compared to those obtained from the Aimsun. For this case study, Aimsun were run 8 times. The traffic flow data used in each simulation are presented in Table 2.

From Figure 9 two main conclusions can be drawn. The first one is that the results obtained in Aimsun for the three sections are quite close to each other, with only slight differences for higher traffic volumes (Simulation 6, 7, and 8). In these simulations, the input traffic flow is very close to or even higher than the capacity of the segments, making traffic flow along the network more unstable.

The second conclusion is that the implemented traffic model (dashed line) does not fit the results obtained by Aimsun, mainly for the speed-density relationship and for the speed-flow rate relationship. However, the flow rate-density relationship shows a good agreement with the results obtained by Aimsun. Herein, it is assumed that as flow rate increases from zero to maximum capacity, speed in the segment remains constant and equal to S_{free}. This assumption is unrealistic, since, with the increase in the flow rate, the interaction between vehicles causes the speed to be reduced. Furthermore, from the flow rate-density and speed-flow rate relationships (Figure 9), it can be seen that the maximum capacity of the segments is greater than the maximum flow rate, q_{max}, defined in Table 1, approximately, 7.6%. For the maximum capacity, the Aimsun features a critical speed, S_{cri}, of, approximately, 98 km/h, and a critical density, ρ_{cri}, of 26 veh/km/lane (speed-density relationship in Figure 9). In addition, it can be observed that the flow rate of the road network does not decrease for higher traffic volumes (Simulation 6,7, and 8). In these situations, Aimsun assumes that the flow rate in the road network is equal to maximum capacity of the segment.

4.2.2 Case study B: Off-ramp segments

Figure 10 compares the traffic model implemented with the data obtained from Aimsun for Sections 1, 2, 3, and 4, respectively. For this case study, Aimsun was run 36 times. The traffic flow data used in each simulation are presented in Table 3.

In the same way as in case study A, the results for these four sections show that the traffic model implemented (dashed line for highway segments and dotted line for off-ramp segment) does not fit the results obtained by Aimsun, presenting significant discrepancies, particularly in the speed-density and the speed-flow rate relationships.

In Figure 10, black dots depicts the results obtained from Section 1; that is, the section that precedes the bifurcation in the network. From this figure, it is possible to observe that the increase in traffic level in the segment South – VFXira has a great impact on the average speed of the section when compared with

the same section of case study A. For example, for simulation 1 in case study B, the average speed in Section 1 is, approximately, 115 km/h for an input flow rate, q_{Input}, of 1650 veh/h ($q_{South-North}$ = 1200 veh/h and $q_{South-VFXira}$ = 450 veh/h), and, for simulation 6, the average speed is, approximately, 80 km/h for an input flow rate, q_{Input}, of 3900 veh/h ($q_{South-North}$ = 1200 veh/h and $q_{South-VFXira}$ = 2700 veh/h). When compared with case study A, the lower speed in Section 1 is, approximately, 98 km/h for flow rates higher than 7200 veh/h.

The brown and light brown dots (Figure 10) illustrate the results obtained for Sections 2, and 3, respectively. That is, the sections that follow the bifurcation in the network. For these two sections the results obtained are similar to the results presented for case study A, as these two sections are found after the bifurcation so only the traffic flow that follows to the North is considered to determine the relations between the three variables. Finally, the blue dots (Figure 10) show the results obtained for the off-ramp segment (Section 4). These results show that according to Aimsun, the limited maximum speed, S_{free}, on the off-ramps is not 60 km/h but, approximately 70 km/h. Secondly, the maximum capacity of 2400 veh/h, i.e. the maximum capacity is, approximately, 2.6 times higher than the maximum capacity initially considered.

4.2.3 Case study C: On-ramp segments

In Figure 11, the traffic model implemented, and the data obtained from Aimsun for Sections 1, 2, 3, and 5 are compared considering 30 Aimsun simulations. The traffic flow data used in each simulation are presented in Table 4.

As in case study A and B, this figure shows that, for these four sections, the traffic model implemented (dashed line for highway segments and dotted line for on-ramp segment) does not fit adequately the results obtained by Aimsun. Sections 1 and 2 are located before the junction of the on-ramp with the main road. These results show that, for high traffic levels on the main road ($q_{South-North}$), simulations 21 to 30, the increase of the traffic flow in segment VFXira – North reduces the flow rate and the speed due to the junction of the two flows. For the $q_{South-North}$ = 7200 veh/h and for high traffic levels in segment VFXira – North, the maximum capacity of these two sections is reduced by, approximately, 300 veh/h/lane. In parallel with these observations, it is possible to verify that the density in these two sections increases with the increase of traffic levels in the segment VFXira – North.

By analysing the results obtained for Section 3, light brown dots in Figure 11, the segment that follows the junction of the two flows, it can be concluded that the limited maximum speed, S_{free}, in this section is not 120 km/h but, approximately, 110 km/h. This, it models the behaviour of the drivers that, when faced with the junction of two flows, tend to reduce their speed slightly as a road safety attitude, even at low traffic levels.

Finally, the green dots in Figure 11 show the results obtained for the on-ramp segment (Section 5). The results are similar to those obtained for the off-ramp: the limited maximum speed, S_{free}, on the on-ramps is not 60 km/h but, approximately 70 km/h; the maximum capacity is only, approximately, 900 veh/h for situations where the traffic level on the main road is high ($q_{South\text{-}North}$ = 3600 – 7200 veh/h); while, for low traffic levels, the maximum capacity is, approximately, 1300 veh/h for $q_{South\text{-}North}$ = 2400 veh/h and 1700 veh/h for $q_{South\text{-}North}$ = 1200 veh/h.

4.2.4 Enhanced traffic model

From the previously presented results, it is possible to conclude that the traffic model implemented, based on the works of Tolba *et al*. (2005) and Fanti *et al*. (2012, 2014), does not fit adequately the results obtained through Aimsun, showing significant differences in the speed-density relationships and in the speed-flow rate relationships. In the following, strategies to reducing these discrepancies will be addressed by introducing two new parameters in the traffic model proposed by Tolba *et al*. (2005): correction factor of the critical density, c_1; and critical speed, S_{cri}. These parameters were estimated from the results obtained by Aimsun, in order to approximate both models.

One of the first conclusions drawn is that the critical density obtained by the microsimulation model for the various sections analysed is higher than the critical density obtained by the implemented traffic model. Critical density, ρ_{cri}, defines the point at which traffic flow evolves from uninterrupted to interrupted. In the traffic model implemented, this point is defined by α_i, as described in Equation 3. A correction factor c_1 was introduced as:

$$\alpha_i = \frac{q_{max,i} \times L_i}{S_{free,i}} \times c_1 = \alpha_i^{theo} \times c_1 \tag{14}$$

c_1 is obtained through ρ_{cri} / $\alpha^{theo}{}_i$, where ρ_{cri} is the average critical density obtained from Aimsun data.

However, increasing α_i, leads to increasing the transition firing speed, $v_i(t)$ (see Equation 1). Therefore, it is needed to correct the transition firing speed, $v_i(t)$. Equation 15 allows to reduce the average flow rate, $q_i(t)$, that leaves from the highway segment i.

$$q_i(t) = v_i(t) \times \frac{q_{max,i}}{q_{max,i}^{theo} \times c_1} \tag{15}$$

where $q_{max,i}$ is the average maximum capacity obtained from Aimsun data and $q^{theo}{}_{max,i}$ the theoretical maximum capacity of the road network (Table 1).

Finally, the last parameter to be introduced in the traffic model is the critical speed, S_{cri}, that is not defined in the traffic model proposed by Tolba *et al*. (2005). Based on the results previously obtained

and in order to simplify the expressions, it was assumed that the speed variation in the uninterrupted flows can be approximated by a linear function, being the critical speed, S_{cri}, is given by:

$$S_{cri} = S_{free} + b \times \alpha_i \tag{16}$$

where b is estimated using linear regression models applied to the results obtained through the microsimulation model. This is introduced by updating Equation 8 to:

$$S_i(t) = \begin{cases} \dfrac{S_{cri} - S_{free}}{\alpha_i} \times m_i^v(t) + S_{free}, & m_i^v(t) \leq \min\left[\alpha_i; C_{i+1} - m_{i+1}^v(t)\right] \\ \dfrac{q_i(t) \times L_i}{m_i^v(t)}, & m_i^v(t) > \min\left[\alpha_i; C_{i+1} - m_{i+1}^v(t)\right] \end{cases} \tag{17}$$

Through the results obtained from the three case studies analysed, it is possible to group the different segments that make up the network into four types:

- Type 1 – contains the generic highway segments and the segments that precede on- and off-ramps (Sections 1 and 2 in the network);
- Type 2 – comprises the segments that follows the junction of the two flows (Section 3 in the network);
- Type 3 – contains the on-ramp segments (Section 5 in the network);
- Type 4 – comprises the off-ramp segments (Section 4 in the network).

In Table 5, the characteristics for the four types of segments are presented, and Figure 12 shows the adjustment of the traffic model proposed to the data obtained from the Aimsun. In Table 5, r^2 is the coefficient of determination from the linear regression equation. For all types of segments, r^2 is closer to 1 (range from 0.77 to 0.96) meaning that the linear model is adequate to describe the speed-density relationship.

In Figure 12, the original model, the enhanced traffic model and the data obtained from the Aimsun for all types of segments are compared. For type 1 segment, Figure 12, only Sections 1, 2, and 3 of case study A were considered as only these result in uninterrupted conditions. From this figure, it is clear that the modified traffic model (black solid line) shows a good agreement with the data obtained from the microsimulation model (black dots). The light brown, green and blue solid lines (Figure 12) show, respectively, the adjustment of the enhanced traffic model to the data obtained from the Aimsun for type 2, type 3, and type 4 segments.

4.3 Validation

For the validation at the macroscopic level, the average speed, density, and flow rate computed from the modified traffic model were compared with the results obtained from Aimsun. In the validation process,

four Origin-Destination matrices (OD) were used (Tables 6 to 9). The Origin-Destination matrix 1 (OD1) is based on real data provided by BRISA (entity responsible for the highways that constitute the network being studied). The remaining OD matrices are linearly proportional to OD1.

In this study, 100 simulations were carried out for each traffic model.

In Tables 10 to 14, the average speed, density, and flow rate computed by the traffic model based on Petri nets is compared with the results obtained through the microsimulation model. Each table presents the data obtained for each section defined in the network (Figure 7). From these results, it is possible to observe that there is a good agreement between the two models. Of the three analysed variables, density presents greater differences obtaining relative errors in the order of 30% for the higher traffic levels. The average speed has average relative errors of less than 20%, while the flow rate has average relative errors of less than 5%.

Tables 15 and 16 compare the flow rates in the bifurcation and in the junction for the four OD matrices, respectively. The main purpose of these two tables is to show that Petri nets are able to model traffic behaviour at the macroscopic level, even in oversaturate conditions. From these results, for all traffic levels, it is clear that there is a good agreement between the two models, presenting low relative errors.

An interesting feature of the proposed methodology is the trade-off between accuracy and simplicity. As expected, the methodology does not describe in detail the behaviour of the vehicles on the freeway, but there is a good agreement between the two methodology. That is, considering the limitation of the model, it is possible to model with accuracy the speed and the flow rate. Demonstrating that the Petri net methodology can be used to monitor simple freeway control systems such as: travel-time predictability, energy consumption, and pollution of the environment. Another advantage of the Petri net model, it is does not suffer from the state explosion problem in cases where traffic is congested. The state size of the problem is the same as in free or congested regime. In addition, it should be mentioned that this methodology does not take into account exceptional events such as accidents or critical weather conditions.

5 Conclusions

In this study, a methodology is proposed to model the traffic behaviour on highway systems from a macroscopic viewpoint, based on continuous times Petri nets. CTPN are an extension of the original Petri nets, in which the marking of a place becomes a non-negative real number and the firing of a transition becomes a continuous flow. The concept of CTPN is used to build a modular model, where the highway network is discretized into smaller segments, based on structural entities (e.g., highway segment, on and off-ramp links).

An initial methodology, based on the works of Tolba *et al*. (2005) and Fanti *et al*. (2012, 2014), was used to model part of the Portuguese Highway network (A1 highway close to Vila Franca de Xira). The results show that this methodology results in inaccurate estimates of key features of the traffic flow. The model in enhanced by including a critical density correction factor and a critical speed, calibrated based on the micro-modelling simulation. This leads to a dramatic increase in the accuracy of the model, allowing its use for predicting traffic flows, as a low computational cost alternative to complex micro-modelling approaches. Due to its low cost, the proposed model is capable of modelling large integrated networks, with limited computational resources, requiring limited calibration for a few key segments.

References

Aimsun (2019). https://www.aimsun.com/. (Page consulted on November 4, 2019).

Alla, H. and David, R. (1998). A modelling and analysis tool for discrete events systems: *Continuous Petri net. Performance Evaluation*, 33(3):175–199.

Cheng, F., Li, H.,Wang, Y., Skitmore, M., and Forsythe, P. (2013). Modeling resource management in the building design process by information constraint Petri nets. *Automation in Construction*, 29:92–99.

David, R. and Alla, H. (2010). *Discrete, Continuous, and Hybrid Petri Nets*. Springer Science & Business Media.

Di Febbraro, A., Giglio, D., and Sacco, N. (2016). A deterministic and stochastic Petri net model for traffic-responsive signaling control in urban areas. *IEEE Transactions on Intelligent Transportation Systems*, 17(2):510–524.

Di Febbraro, A. and Sacco, N. (2004). On modelling urban transportation networks via hybrid Petri nets. *Control Engineering Practice*, 12(10):1225–1239.

Di Febbraro, A. and Sacone, S. (1998). Hybrid Petri nets for the performance analysis of transportation systems. In *Proceedings of the 37th IEEE Conference on Decision and Control (Cat. No. 98CH36171)*, volume 3, pages 3232–3237. IEEE.

Dotoli, M. and Fanti, M. P. (2006). An urban traffic network model via coloured timed Petri nets. *Control Engineering Practice*, 14(10):1213–1229.

Dotoli, M., Fanti, M. P., and Iacobellis, G. (2011). A freeway traffic control model by first order hybrid Petri nets. In *2011 IEEE International Conference on Automation Science and Engineering*, pages 425–431. IEEE.

Eisenberger, D. and Fink, O. (2017). Assessment of maintenance strategies for railway vehicles using Petri-nets. *Transportation Research Procedia*, 27:205–214.

Fanti, M., Iacobellis, G., Mangini, A., and Ukovich, W. (2014). Freeway traffic modeling and control in a first-order hybrid Petri net framework. *IEEE Transactions on Automation Science and Engineering*, 11(1):90–102.

Fanti, M. P., Mangini, A. M., Giorgio, I., and Ukovich, W. (2012). A freeway traffic model in a first order hybrid Petri net framework. In *9th International Conference on Modeling, Optimization & SIMulation*.

Ferrara, A., Sacone, S., and Siri, S. (2018). *Freeway traffic modelling and control*. Springer.

Ferreira, C., Canhoto Neves, L., Silva, A., and de Brito, J. (2019). Stochastic maintenance models for ceramic claddings. *Structure and Infrastructure Engineering*.

Giua, A. (1991). Traffic light controller based on Petri nets. Technical report, Rensselaer Polytechnic Institute.

HCM (2010). Highway capacity manual. Technical report, Transportation Research Board.

Herajy, M., Liu, F., Rohr, C., and Heiner, M. (2018). Coloured hybrid Petri nets: An adaptable modelling approach for multi-scale biological networks. *Computational biology and chemistry*, 76:87–100.

Jensen, K. (1986). Colored Petri nets: control models and their properties. *Lecture notes in computer science*, 254(Part 1).

Julvez, J. J. and Boel, R. K. (2010). A continuous Petri net approach for model predictive control of traffic systems. *IEEE Transactions on Systems, Man, and Cybernetics-Part A: Systems and Humans*, 40(4):686–697.

Kim, S.-y. and Yang, Y. (2018). A self-navigating robot using fuzzy Petri nets. *Robotics and Autonomous Systems*, 101:153–165.

Latorre-Biel, J.-I., Faulin, J., Jiménez, E., and Juan, A. A. (2017). Simulation model of traffic in smart cities for decision-making support: Case study in Tudela (Navarre, Spain). In *International Conference on Smart Cities*, pages 144–153. Springer.

Murata, T. (1989). Petri nets: Properties, analysis and applications. In *Proceedings of the IEEE*.

Peterson, J. L. (1977). Petri nets. *Computing Surveys*, 9(3):223–252.

Schneeweiss, W. G. (2004). *Petri Net Picture Book: An elementary introduction to the best pictorial description of temporal changes*. LiLoLe - Verlag GmbH.

Si, Y.-W., Chan, V.-I., Dumas, M., and Zhang, D. (2018). A Petri nets based generic genetic algorithm framework for resource optimization in business processes. Simulation Modelling Practice and Theory, 86:72–101.

Tolba, C., Lefebvre, D., Thomas, P., and El Moudni, A. (2005). Continuous and timed Petri nets for the macroscopic and microscopic traffic flow modelling. *Simulation Modelling Practice and Theory*, 13(5):407–436.

Toledo, T., Koutsopoulos, H., Davol, A., Ben-Akiva, M., Burghout, W., Andréasson, I., Johansson, T., and Lundin, C. (2003). Calibration and validation of microscopic traffic simulation tools: Stockholm case study. *Transportation Research Record: Journal of the Transportation Research Board*, 1831:65–75.

Zhang, L.-G., Li, Z.-L., and Chen, Y.-Z. (2008). Hybrid Petri net modeling of traffic flow and signal control. In *2008 International Conference on Machine Learning and Cybernetics*, volume 4, pages 2304–2308. IEEE.

Table 1 – Network characteristics

Section	Type	Length [m]	S_{free} [km/h]	q_{max} [veh/h]	Number of lanes	ρ_{max} [veh/km]
1	Highway	341.1	120	2400	3	150
2	Highway	245.4	120	2400	3	150
3	Highway	194.9	120	2400	3	150
4	Off-ramp	178.5	60	900	1	150
5	On-ramp	218.4	60	900	1	150

Table 2 – Input traffic flow [veh/h] data used in each simulation for the case study A

Simulation	1	2	3	4	5	6	7	8
$q_{South\text{-}North}$	1200	2400	3600	4800	6000	7200	8400	9600

Table 3 – Input traffic flow [veh/h] data used in each simulation for the case study B

Simulation	1	2	3	4	5	6	7	8	9	10	11	12
$q_{South\text{-}North}$	1200						2400					
$q_{South\text{-}VFXira}$	450	900	1350	1800	2250	2700	450	900	1350	1800	2250	2700
Simulation	13	14	15	16	17	18	19	20	21	22	23	24
$q_{South\text{-}North}$	3600						4800					
$q_{South\text{-}VFXira}$	450	900	1350	1800	2250	2700	450	900	1350	1800	2250	2700
Simulation	25	26	27	28	29	30	31	32	33	34	35	36
$q_{South\text{-}North}$	6000						7200					
$q_{South\text{-}VFXira}$	450	900	1350	1800	2250	2700	450	900	1350	1800	2250	2700

Table 4 – Input traffic flow [veh/h] data used in each simulation for the case study C

Simulation	1	2	3	4	5	6	7	8	9	10
$q_{South\text{-}North}$			1200					2400		
$q_{VFXira\text{-}North}$	450	900	1350	1800	2250	450	900	1350	1800	2250
Simulation	11	12	13	14	15	16	17	18	19	20
$q_{South\text{-}North}$			3600					4800		
$q_{VFXira\text{-}North}$	450	900	1350	1800	2250	450	900	1350	1800	2250
Simulation	21	22	23	24	25	26	27	28	29	30
$q_{South\text{-}North}$			6000					7200		
$q_{VFXira\text{-}North}$	450	900	1350	1800	2250	450	900	1350	1800	2250

Table 5 – Type segment characteristics

Variable	Type 1	Type 2	Type 3	Type 4
S_{free} [km/h]	122.30	109.43	66.96	71.67
ρ_{cri} [veh/km]	25.68	28.16	14.60	39.12
q^{theo}_{max} [veh/h]	2400	2400	900	900
q_{max} [veh/h]	2581.37	2538.81	900.22	2304.06
c_1 [-]	1.31	1.28	1.09	3.12
α [veh/km]	25.38	28.16	14.06	39.12
b [-]	-0.88	-0.63	-0.29	-0.31
S_{cri} [km/]	99.66	91.80	62.77	59.47
r^2 [-]	0.95	0.83	0.77	0.96

Table 6 – Origin-Destination matrix 1 (OD1)

	VFXira	North	Total
South	772	1263	2035
VFXira	-	294	294
Total	772	1557	2329

Table 7 – Origin-Destination matrix 2 (OD2)

	VFXira	North	Total
South	1544	2526	4070
VFXira	-	588	588
Total	1544	3114	4658

Table 8 – Origin-Destination matrix 3 (OD3)

	VFXira	North	Total
South	2316	3789	6105
VFXira	-	882	882
Total	2316	4671	6987

Table 9 – Origin-Destination matrix 4 (OD4)

	VFXira	North	Total
South	3088	5052	8140
VFXira	-	1176	1176
Total	3088	6228	9316

Table 10 – Comparison of the fundamental parameters in Section 1

	Aimsun			Petri nets			Relative error [%]		
	Speed	Density	Flow rate	Speed	Density	Flow rate	Speed	Density	Flow rate
OD1	111.6	6.1	2026.5	117.4	5.6	2036.5	5.2	9.1	0.5
OD2	105.7	13.1	4064.8	112.5	11.1	4072.9	6.4	14.9	0.2
OD3	91.2	24.3	6092.4	105.8	17.0	6109.2	16.0	30.0	0.3
OD4	86.5	30.7	7418.8	86.2	27.6	7746.9	0.4	10.1	4.4

Table 11 – Comparison of the fundamental parameters in Section 2

	Aimsun			Petri nets			Relative error [%]		
	Speed	Density	Flow rate	Speed	Density	Flow rate	Speed	Density	Flow rate
OD1	116.3	3.6	1257.3	119.2	3.4	1263.1	2.5	5.1	0.5
OD2	113.6	7.5	2523.1	116.2	6.9	2526.3	2.2	7.6	0.1
OD3	109.0	11.6	3785.2	113.0	10.5	3839.1	3.7	10.1	1.4
OD4	102.6	16.5	5044.8	110.0	13.9	5115.2	7.2	15.2	1.4

Table 12 – Comparison of the fundamental parameters in Section 3

	Aimsun			Petri nets			Relative error [%]		
	Speed	Density	Flow rate	Speed	Density	Flow rate	Speed	Density	Flow rate
OD1	107.2	4.8	1551.7	106.5	4.7	1556.3	0.7	0.6	0.3
OD2	103.1	10.3	3107.0	103.5	9.5	3112.7	0.4	7.8	0.2
OD3	95.6	18.7	4660.7	100.4	14.4	4718.4	5.1	23.0	1.2
OD4	91.1	27.1	6004.1	97.8	18.5	6088.2	7.4	31.6	1.4

Table 13 – Comparison of the fundamental parameters in Section 4

	Aimsun			Petri nets			Relative error [%]		
	Speed	Density	Flow rate	Speed	Density	Flow rate	Speed	Density	Flow rate
OD1	68.0	11.4	767.5	68.3	10.8	771.9	0.5	5.4	0.6
OD2	64.6	24.0	1538.2	65.0	21.5	1543.7	0.6	10.2	0.4
OD3	59.1	39.0	2301.7	61.8	31.6	2265.6	4.5	19.0	1.6
OD4	58.4	40.6	2367.4	60.2	36.6	2626.0	3.1	9.7	10.9

Table 14 – Comparison of the fundamental parameters in Section 5

	Aimsun			Petri nets			Relative error [%]		
	Speed	Density	Flow rate	Speed	Density	Flow rate	Speed	Density	Flow rate
OD1	65.3	4.6	295.4	65.7	4.4	294.2	0.7	3.6	0.4
OD2	64.0	9.2	586.1	64.4	8.8	588.3	0.7	4.8	0.4
OD3	51.0	22.4	879.6	55.2	16.1	882.2	8.4	28.2	0.3
OD4	8.6	132.3	965.5	6.9	139.9	976.7	20.4	5.8	1.2

Table 15 – Comparison of the flow rate [veh/h] in the bifurcation

	Aimsun			Petri nets			Relative error [%]		
	South	North	VFXira	South	North	VFXira	South	North	VFXira
OD1	2026.5	1258.2	768.2	2036.5	1263.9	772.6	0.5	0.5	0.6
OD2	4064.8	2525.0	1539.7	4072.9	2527.9	1545.0	0.2	0.1	0.3
OD3	6092.4	3788.2	2304.0	6109.2	3841.7	2267.5	0.3	1.4	1.6
OD4	7418.8	5048.9	2369.8	7746.9	5118.7	2628.2	4.4	1.4	10.9

Table 16 – Comparison of the flow rate [veh/h] in the junction

	Aimsun			Petri nets			Relative error [%]		
	South	North	VFXira	South	North	VFXira	South	North	VFXira
OD1	1257.3	294.4	1552.7	1263.1	294.2	1557.2	0.5	0.4	0.3
OD2	2523.1	586.1	3109.1	2526.3	588.3	3114.6	0.1	0.4	0.2
OD3	3785.2	879.6	4664.6	3839.1	882.2	4721.3	1.4	0.3	1.2
OD4	5044.8	965.5	6009.8	5115.2	976.7	6091.9	1.4	1.2	1.4

Figures caption

Figure 1 – Example of a transition (firing) rule (adapted from Murata, 1989): (a) marking before transition t_1 fires; (b) marking after transition t_1 fires

Figure 2 – Petri net scheme for a generic highway segment (adapted from Tolba *et al*., 2005 and Fanti *et al*., 2014)

Figure 3 – Petri net scheme for the origin segment

Figure 4 – Petri net scheme for the on-ramp (adapted from Fanti *et al*., 2014)

Figure 5 – Petri net scheme for the off-ramp (adapted from Fanti *et al*., 2014)

Figure 6 – Petri net scheme for the destination segment

Figure 7 – Location of the network

Figure 8 – Petri net scheme of the traffic model for the network

Figure 9 – Comparison of the relationships between speed, density, and flow rate between the Petri net model and the data obtain from the Aimsun – Case study A

Figure 10 – Comparison of the relationships between speed, density, and flow rate between the Petri net model and the data obtain from the Aimsun – Case study B

Figure 11 – Comparison of the relationships between speed, density, and flow rate between the Petri net model and the data obtain from the Aimsun – Case study C

Figure 12 – Adjustment of the Petri net model to the data obtained from the Aimsun for type 1 segment (Sections 1, 2, and 3 of the case study A), type 2 segment (Section 3 of the case study C), type 3 segment (Section 5 of the case study C), and type 4 segment (Section 4 of the case study B)

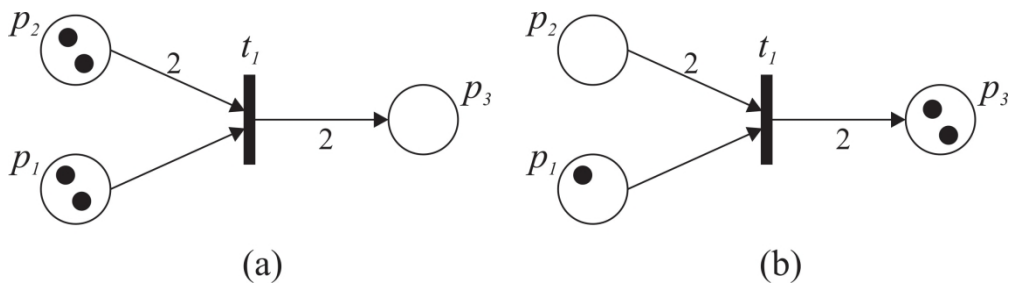

Example of a transition (firing) rule (adapted from Murata, 1989): (a) marking before transition t1 fires; (b) marking after transition t1 fires

958x259mm (72 x 72 DPI)

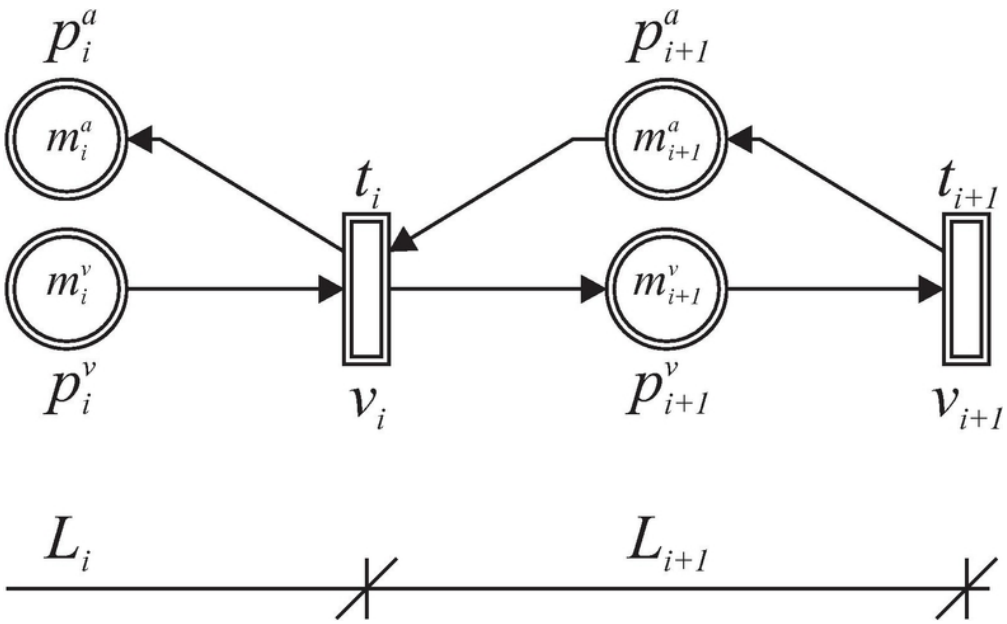

Petri net scheme for a generic highway segment (adapted from Tolba et al., 2005 and Fanti et al., 2014)

66x40mm (300 x 300 DPI)

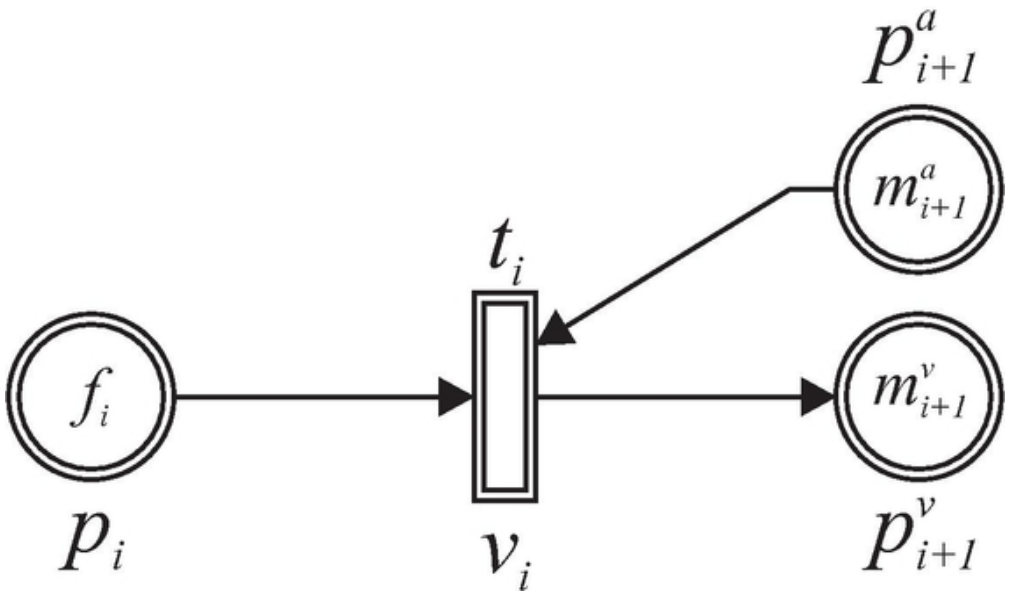

Petri net scheme for the origin segment

48x28mm (300 x 300 DPI)

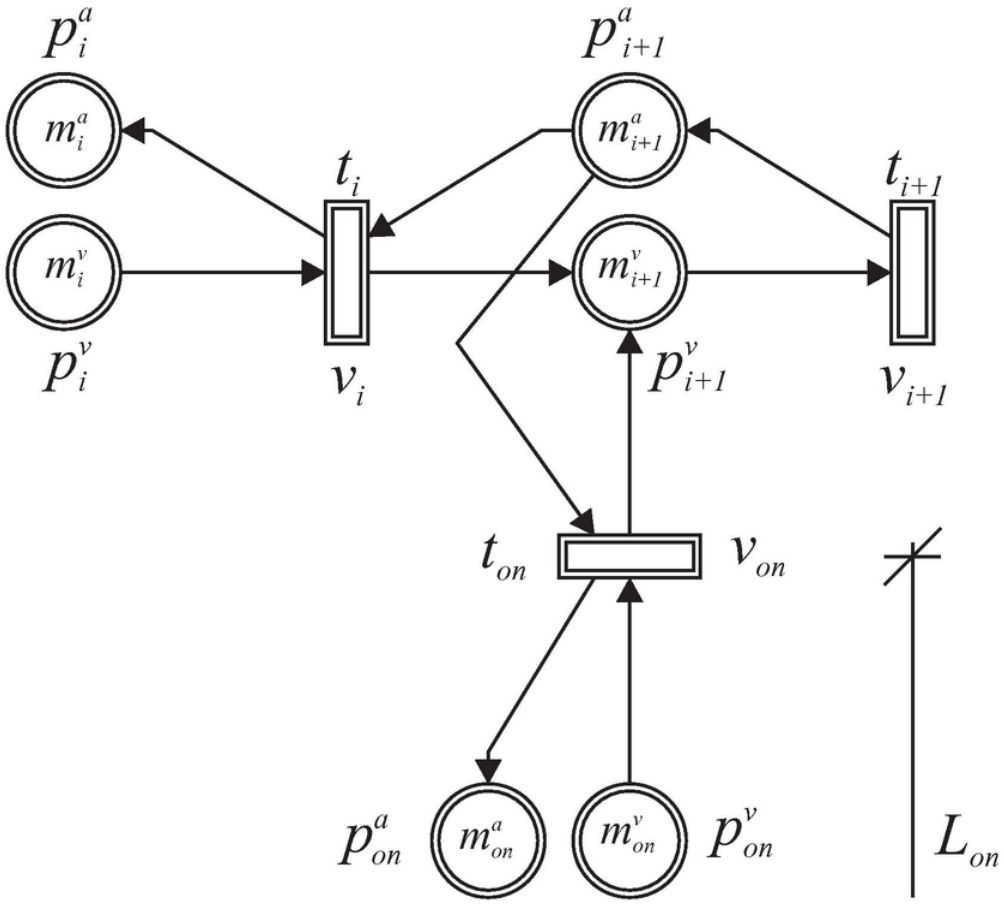

Petri net scheme for the on-ramp (adapted from Fanti et al., 2014)

70x63mm (300 x 300 DPI)

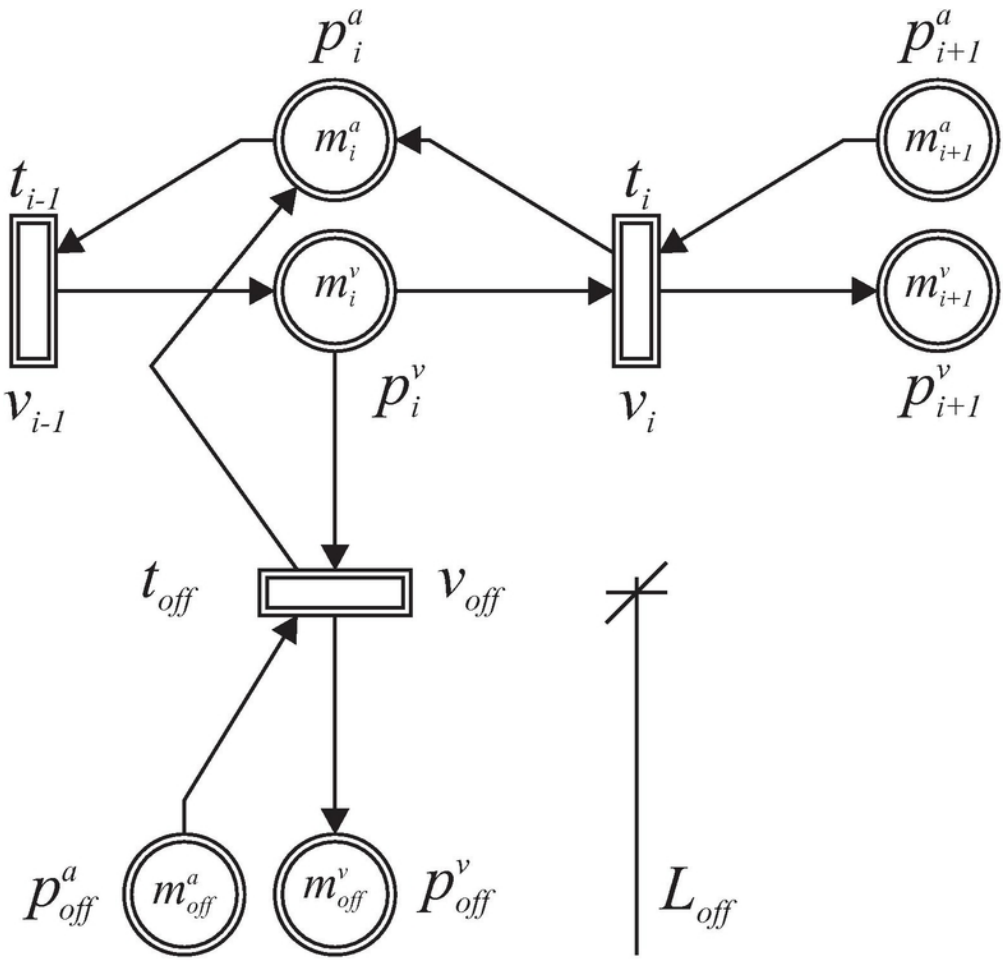

Petri net scheme for the off-ramp (adapted from Fanti et al., 2014)

66x63mm (300 x 300 DPI)

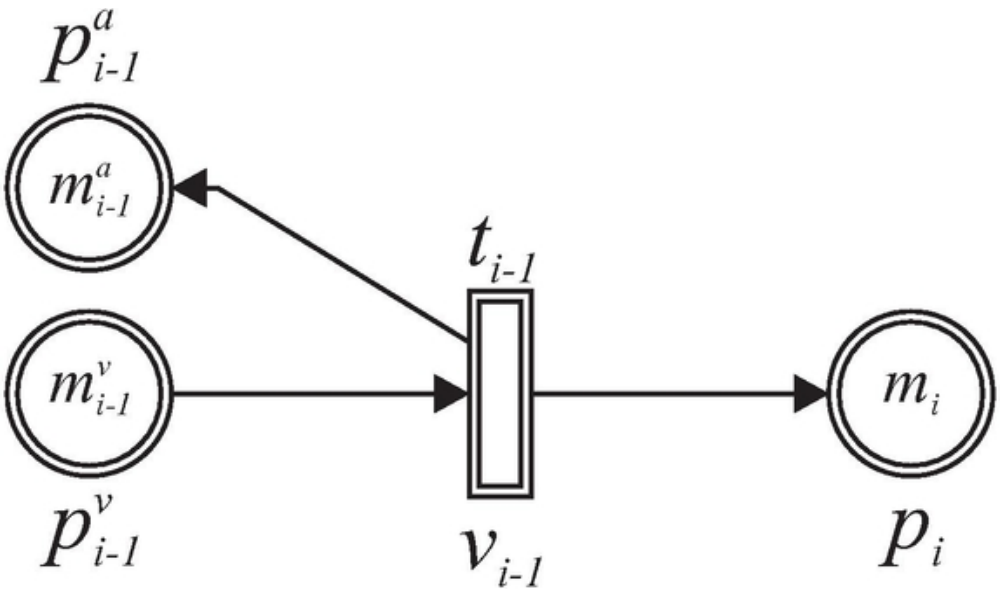

Petri net scheme for the destination segment

48x28mm (300 x 300 DPI)

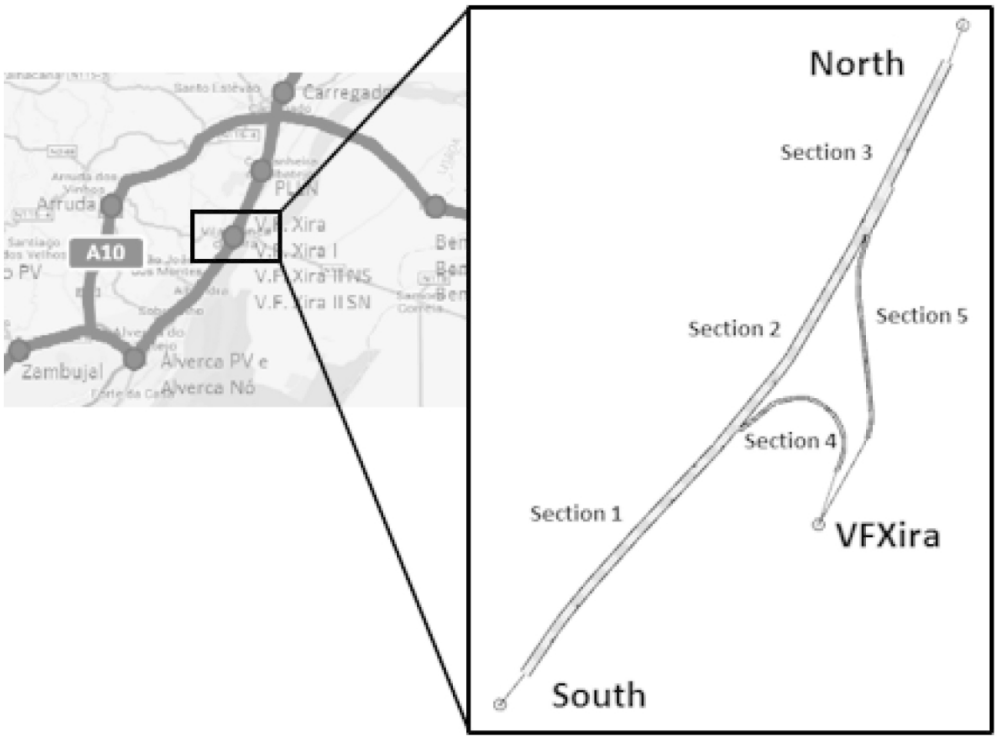

Location of the network

915x683mm (72 x 72 DPI)

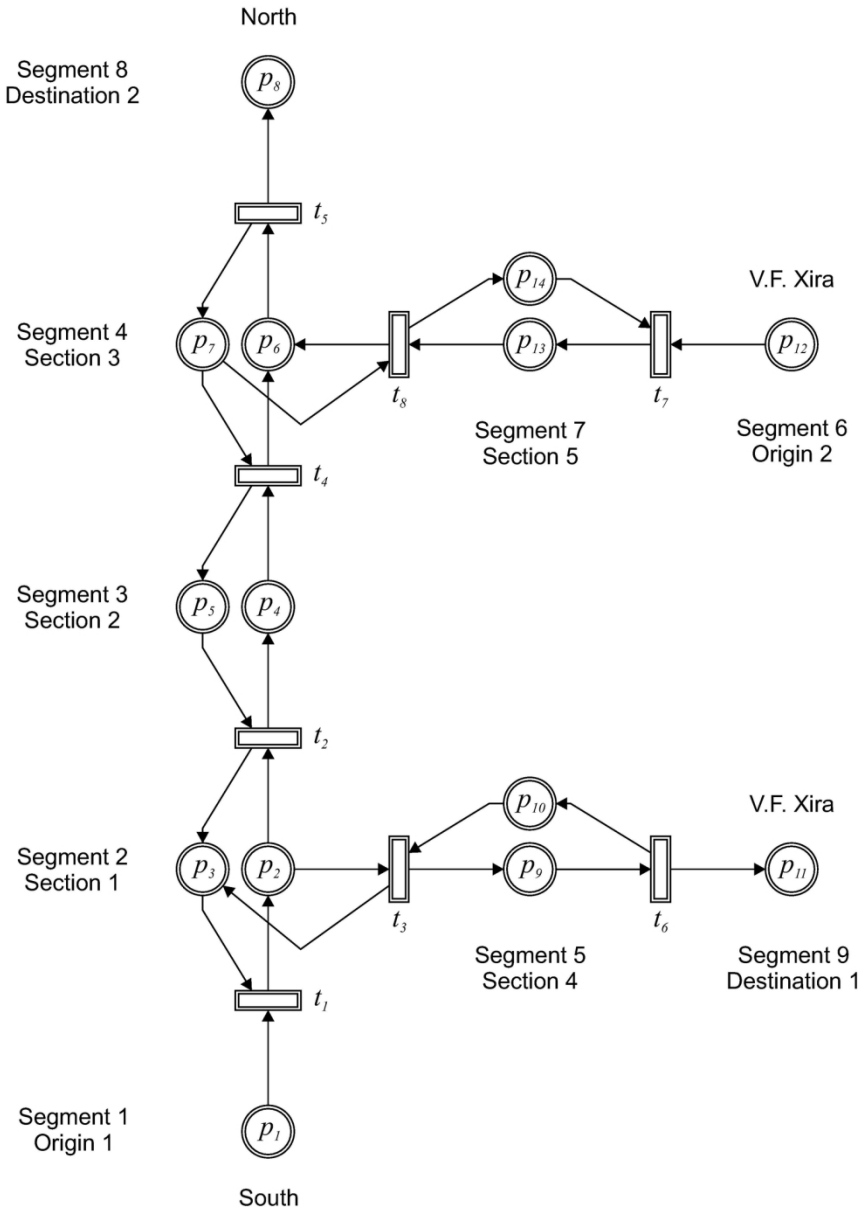

Petri net scheme of the traffic model for the network

130x183mm (300 x 300 DPI)

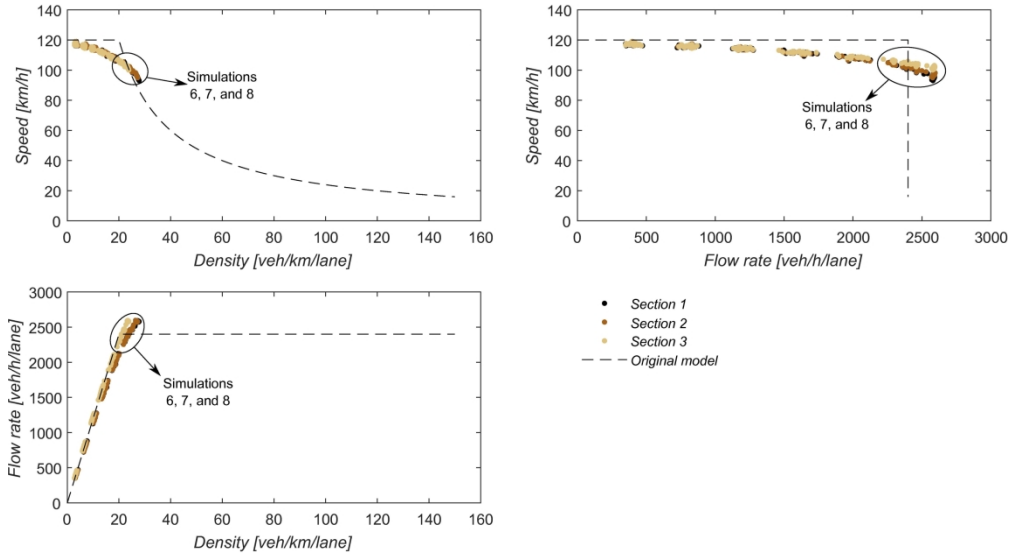

Comparison of the relationships between speed, density, and flow rate between the Petri net model and the data obtain from the Aimsun – Case study A

234x128mm (300 x 300 DPI)

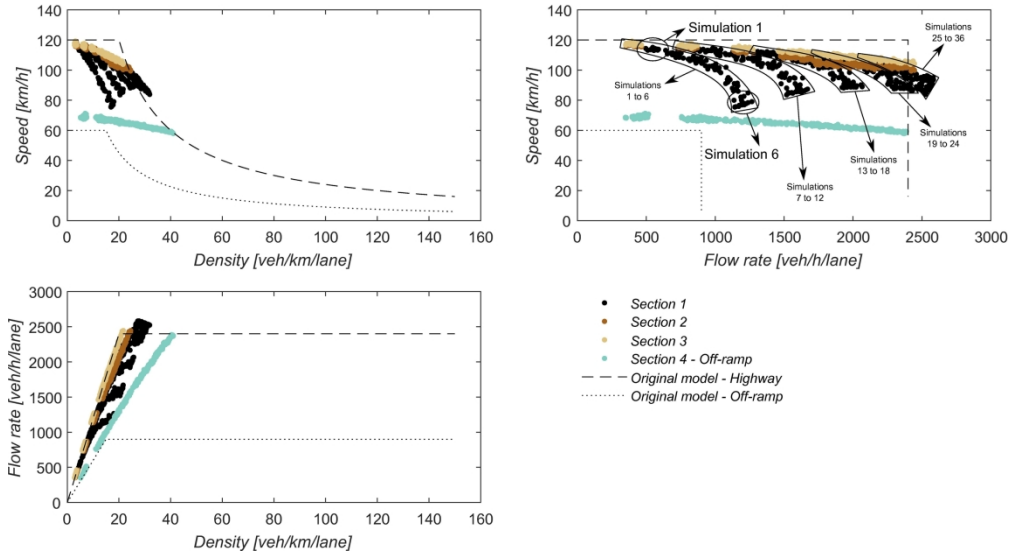

Comparison of the relationships between speed, density, and flow rate between the Petri net model and the data obtain from the Aimsun – Case study B

234x128mm (300 x 300 DPI)

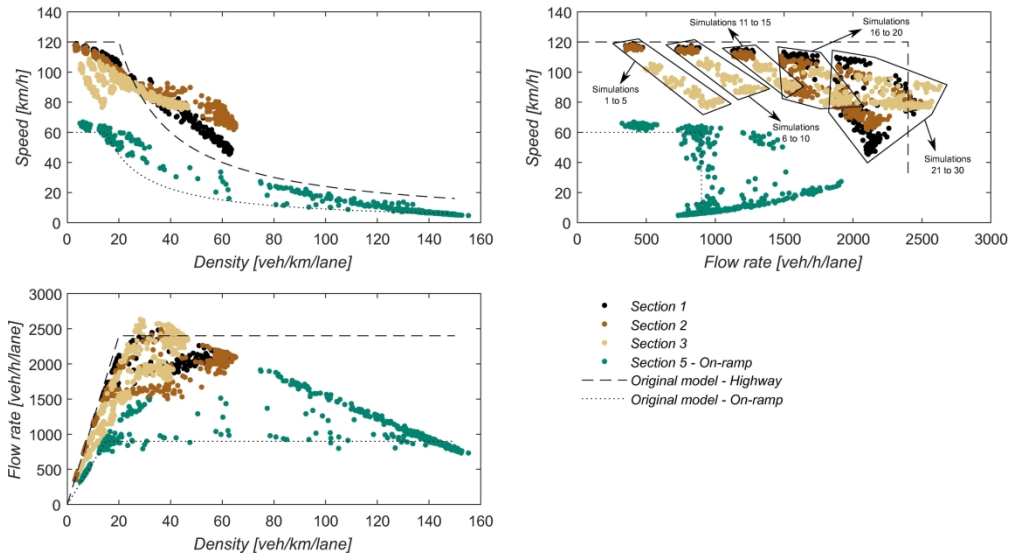

Comparison of the relationships between speed, density, and flow rate between the Petri net model and the data obtain from the Aimsun – Case study C

234x128mm (300 x 300 DPI)

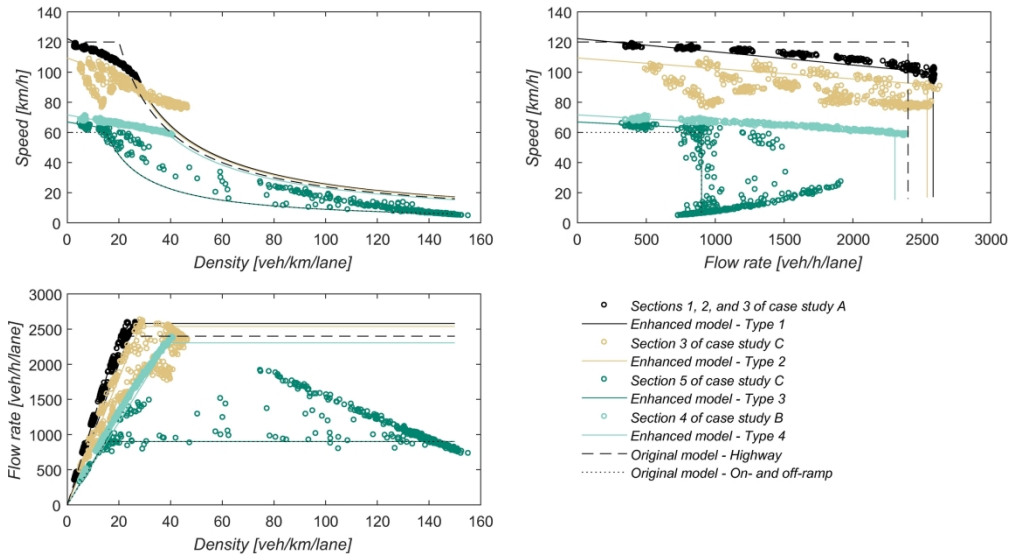

Adjustment of the Petri net model to the data obtained from the Aimsun for type 1 segment (Sections 1, 2, and 3 of the case study A), type 2 segment (Section 3 of the case study C), type 3 segment (Section 5 of the case study C), and type 4 segment (Section 4 of the case study B)

234x128mm (300 x 300 DPI)